The effect of activation energy on gaseous detonation initiation and propagation in curved geometries

Carlos Chiquete and Mark Short
Los Alamos National Laboratory
Los Alamos, NM, USA

1 Introduction

Detonations in gaseous mixtures typically manifest as hydrodynamically unstable waves where multiple transverse shock waves transit across the leading detonation front [5], continually accelerating and decelerating the flow but achieving self-sustained supersonic propagation of the wave. Our main insights into the mechanisms promoting initiation and propagation of these waves is often derived from experiments and simulations in simplified channel or tube confined geometries. Linear stability analyses [4, 14] (i.e. mapping of stability boundaries) have established how certain parameters promote instability (i.e. growth rate, frequency and including appearance of multiple unstable modes) including the activation energy for the idealized one-step Arrhenius rate for instance. Relatedly, Lont et al. [6] have more recently quantified how increasing activation energy generates ever larger departures from Chapman-Jouguet (CJ) flow conditions (including front normal detonation wave velocity, curvature, reaction strength and acceleration) as the cellular wave propagates in rigid channels. Recently, stable non-cellular propagating detonations were observed for a weakly unstable mixture [1, 2, 13] across three different geometries which impart significant global wave curvature on the lead shock front (i.e. compliant boundary channel, rigid 2D arc, and rigid spherical shell geometries). Global curvature was thus shown to have a dramatic effect on the position of the neutral stability boundaries (and thus the detonation flow configuration) as this model otherwise produces regular cellular detonation propagation in the familiar rigid channel geometry. This was true both in the arc and spherical shell geometries which showed consistent laminar behavior for similar inner and outer radii – even with the unsteady dynamics and geometric convergence at the equator specific to the spherical geometry [1].

There is, however, an additional, open question only partially investigated in Short et al. [13] concerning the possible effects of global curvature on more realistic (i.e. more irregular cellular mixtures) that are likely to be encountered in applications. It was found that the stabilized or laminar flow propagation state was absent in 2D arcs when the activation energy was increased for an equivalently-scaled geometry and cellular propagation was re-established. Additionally, a limited decoupling of wave front and following reaction was observed near the inner region when the inner radius is reduced due to the increased state sensitivity of the Arrhenius reaction rate. This latter observation was deemed consistent with a sequence of experimental and numerical studies [8] that have shown the the criticality of the inner radius in establishing a fully attached cellular flow across the explosive region. Here, we investigate whether the addition of the spherical front curvature component would promote or delay the onset of

Correspondence to: chiquete@lanl.gov

initiation failure and propagation for a more unstable mixture. As a starting point then, the first phase of this investigation is a comparison of the wave initiation process as a function of activation energy in either curved, confining geometry. Now, previous work investigating the direct initiation of detonation using multi-step reaction schemes [9] suggests more energy is required to ignite the mixture as the dimensionality is increased from planar, cylindrical and spherical initiation at least when mixtures tend to produce stable (or regular) propagation. However, this general viewpoint is modified when the effects of heightened detonation instability can modify the simple picture built up from simple blast theories (which do rely on a steady wave assumption for example). These results also reflect dynamics specific to initiation "kernels" that are isolated in space and then can then freely propagate to ultimately limit to a planar flow.

In the present work, we are interested in placing the initiation kernel in a more relevant geometry for applications where detonation waves must interact or reflect off rigid boundaries and then potentially progress to a detonation wave that transits or diffracts around the curved explosive geometry (i.e. rotating detonation engines and related propulsion concepts [12]). Given the curved geometric setting, this process must then necessarily impart a broad global curvature of the front throughout this initiation and propagation phase and we are interested in its interaction with variations of the applied activation energy and therefore, influence of the strength and irregularity of the corresponding detonation instability. Therefore, this latter setting differs significantly with these previous studies [3, 9] – further motivating our current investigation.

2 Numerical models and methods

Consistent with the prior studies we use the reactive Euler equations and an idealized mixture constitutive model, with ideal gas equation-of-state and one-step Arrhenius kinetics,

$$\frac{D\rho}{Dt}+\rho\nabla\cdot\mathbf{u}=0,\frac{D\mathbf{u}}{Dt}=-\frac{1}{\rho}\nabla p,\frac{De}{Dt}=\frac{p}{\rho^2}\frac{D\rho}{Dt},e=\frac{p}{(\gamma-1)\rho}-Q\lambda,\frac{D\lambda}{Dt}=k(1-\lambda)\exp(-E/(p/\rho)). \tag{1}$$

where we have used a non-dimensionalization of density ρ, pressure p, particle velocity vector $\mathbf{u}$ and specific internal energy e, total derivative denoted by $D/Dt = \partial/\partial t + \mathbf{u}\cdot\nabla$. A standard non-dimensionalization has been applied here to our governing equations, dimensional variables and parameters and is based on quiescent flow pressure and density variables. Parameters include the adiabatic expansion exponent γ, heat release parameter Q and the activation energy parameter E. For the kinetics, these depend on a reaction progress variable λ and reaction kinetic pre-factor k. The length and time scales are based on the half-reaction length in the ZND flow for the mixture. Details are provided in the related studies (e.g [13]) and omitted here for brevity. The kinetic constant k is set so that the half-reaction zone length corresponds to a unit length of 1 in the transformed coordinate system. We set $\gamma = 1.2$, $Q = 50$, and therefore $D_{CJ} \approx 6.8095$. For the reaction rate, we use $k \approx 3.6407$ for $E = 10$, $k \approx 7.6648$ for $E = 15$ and $k \approx 16.4397$ for $E = 20$ in order to satisfy the half-reaction zone scaling. The ZND solutions in Fig. 1(a) show how increases in E lead to greater reaction nearer to the front.

The numerical methods are as described previously in our related studies [1, 2, 13]. To briefly summarize these, the present calculations take place on a Cartesian mesh with a cell-centered finite volume scheme [11]. Two levels of block-structured adaptive mesh refinement [10] are used, with a refinement factor of 4. The simulations explored here use 20 points per unit half-reaction-zone length at the finest scale. Previous and current convergence studies show that the computational results are independent of mesh size at these resolutions. The relevant diagnostics here is a weighted pressure gradient imaging function that we have previously applied to visualize the main flow structures as the detonation propagates through our chosen geometries. The computational geometries investigated in this work are

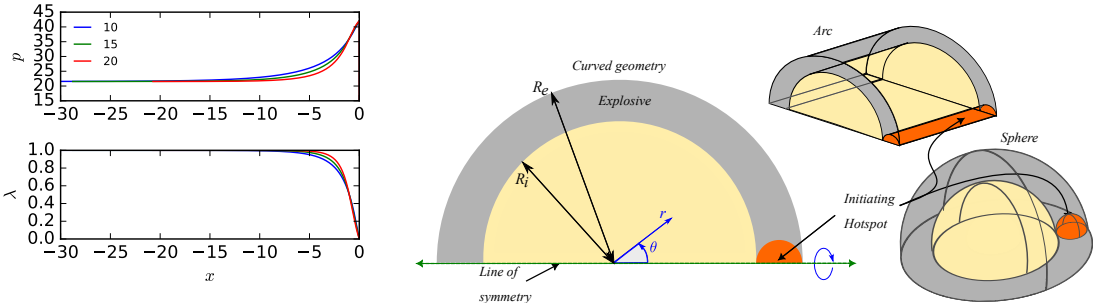

Figure 1: (a) The ZND flow solution as function of activation energy for our present idealized model as function as distance from the shock x. (b) The curved geometry setup parameterized by the inner and outer radius. The spherical and 2D arc geometries are also shown in perspective. Note that the 2D arc extends indefinitely in the orthogonal direction to the $r - \theta$ plane.

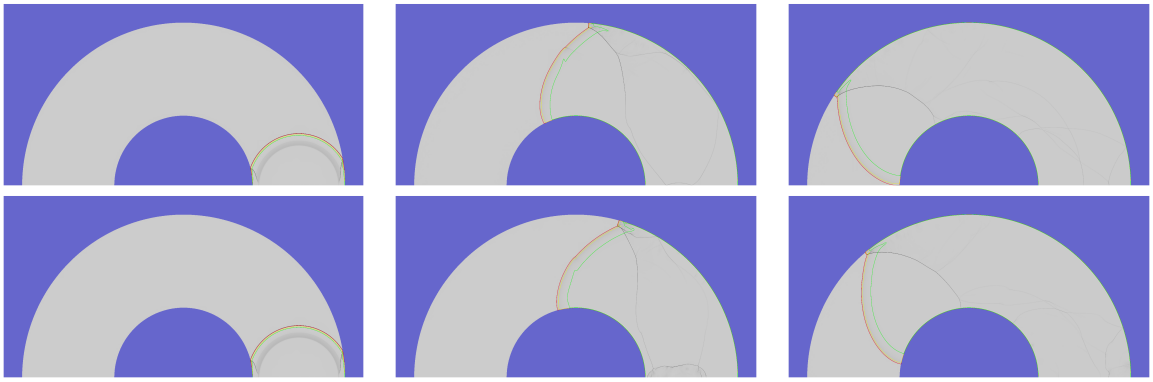

Figure 2: The evolution of the 2D arc (top row) and spherical geometry (bottom row) with $R_i = 75$ and $R_e = 175$ with $E = 10$. The red line represents 1% reaction, yellow is 50% and green is 99%.

diagrammed in Fig. 1(b). The curved geometry includes the 2D planar arc geometry previously studied in [13] and a more recently studied spherical shell geometry [1] when a polar symmetry condition is applied to the half-circle geometry shown in the figure. In either case, the calculations are two-dimensional (2D) and take place in the Cartesian mesh. The inner and outer boundaries are rigid. In our convention, the radial distance is denoted by r and θ is the azimuthal angle. For the 2D arc geometry, the results are considered invariant in the axial coordinate and for the spherical shell results, it is assumed that there is a symmetry in the polar angle coordinate. Figure 1(b) also makes clear the initiation of the wave proceeds via a "hot spot'" spanning the thickness of the explosive region and filled with the CJ state pressure, density and therefore temperature (and zero flow velocity). As such, the energy embedded in each hot spot is equivalent for as the activation energy is increased but not comparing across geometry for a set activation energy due to the difference in dimensionality.

3 Results and analysis

As a reference point for the higher activation energy mixture results, Fig. 2 shows the evolution of the wave from the initial hotspot for both the arc and spherical geometries for $E = 10$ for $R_i = 75$ and $R_e = 175$. Gray regions represent the extent of the explosive region, dark regions of the flow represent large pressure gradients and colored lines represent partially reacted contours in the flow. The evolution

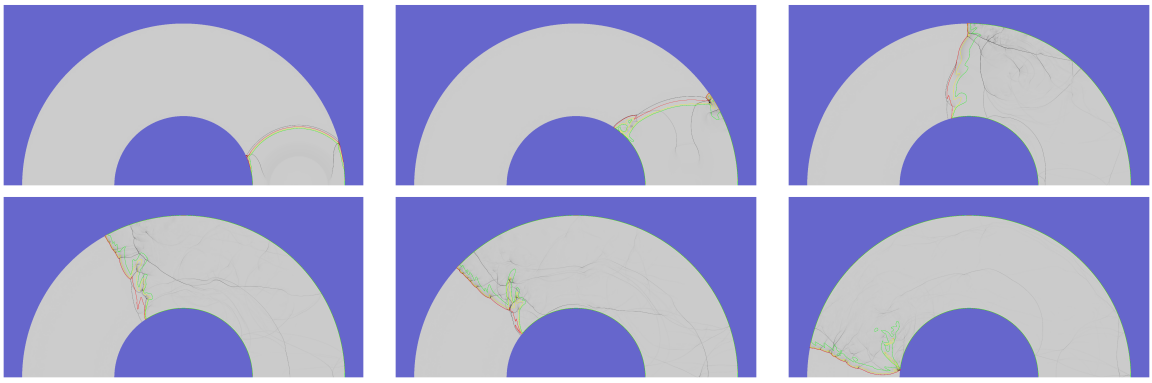

Figure 3: The evolution of the 2D arc geometry with $E = 15$. Geometry and contours as in Fig. 2.

is quite similar between the geometries with the detonation wave forming almost immediately across the explosive and remains attached throughout (as evidenced by the consistent distance between the reaction contours shown in the figure). Both cases show the existence of a small region on the outer arc where the structure is dominated by a cellular instability which does not penetrate the interior of the explosive region. However, in the interior we see the appearance of a broadly laminar flow previously studied by these authors [1, 2, 13] for this same activation energy. Again, the two geometries see a consistent flow structure independently of the dimensionality of the curved geometry. More importantly for our focused investigation here, it can be seen that the initial kernel has the required energy to set off a detonation almost immediately for this activation energy in both geometries.

Moving to $E = 15$, the reaction zone becomes thinner for the ZND planar wave (see Fig. 1(a)) and the temperature sensitivity is ratcheted up in the reaction rate. As a result, we see the results shown in Fig. 3 for $R_i = 75$ and $R_e = 175$, firstly for the arc geometry. The reaction is not nearly as prompt as in the $E = 10$ case shown in the top row of Fig. 2. The initiation kernel is almost able to generate a detonation wave across the whole explosive region as in $E = 10$ but it does struggle to fully establish. The first two panels also show the formation of two transverse shockwaves and their propagation inward into a mostly coupled shock and reactive flow. However, the interior features the most curvature and becomes clear that the inner transverse wave does not survive for long and you begin to see a disassociated flow there where the lead shock becomes detached from the following reaction zone. It also is clear from these panels that the outer transverse wave arrives in the interior to ignite the flow and recouple the lead front with the reaction behind. There is also a region of not fully burnt reactants that hang close to the lead reactive wave and persists to the symmetry line. The near-contour interior region seems sluggish even so in fully reacting the flow and seems to lag behind the interior instead of leading it. This is consistent with the previous behavior observed in Ref. [13]. Again, for the $E = 10$ case, the initiation kernel is enough to establish the wave and the transverse shock initiation is not needed in the end.

Moving to the spherical geometry results in Fig. 4, there is a far more sluggish initiation process than in the $E = 10$ (bottom row of Fig. 2) as may be expected. However, the differences are more pronounced than in the arc case in a few respects. Here, the only coupled shock/reaction zone structure is actually firmly attached to the outer contour – there is hardly any coupling in the interior. The partially unburnt pocket persists well behind the lead shock and reactive region. The transverse wave nevertheless does arrive in time to ignite the whole explosive region before hitting the symmetry line. Interestingly, there is a subtle difference after the wave establishes. The arc case shows an increase in lag in the wave attached to the inner contour and an unreacted pocket is attached to the front near the inner contour throughout. Here, the spherical case basically leads from this interior contour and the unreacted pocket is no longer attached. Therefore, there is an interesting possibility the spherical convergence at the

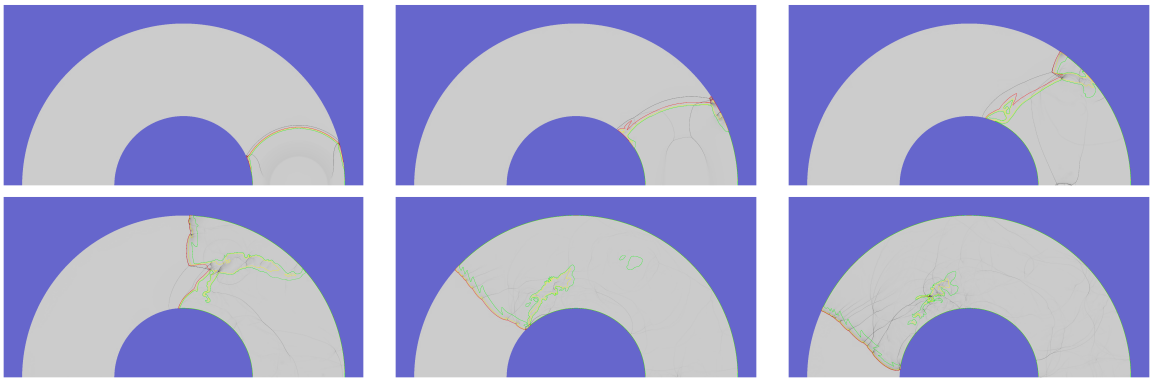

Figure 4: The evolution of the spherical geometry with $E = 15$. Geometry and contours as in Fig. 2.

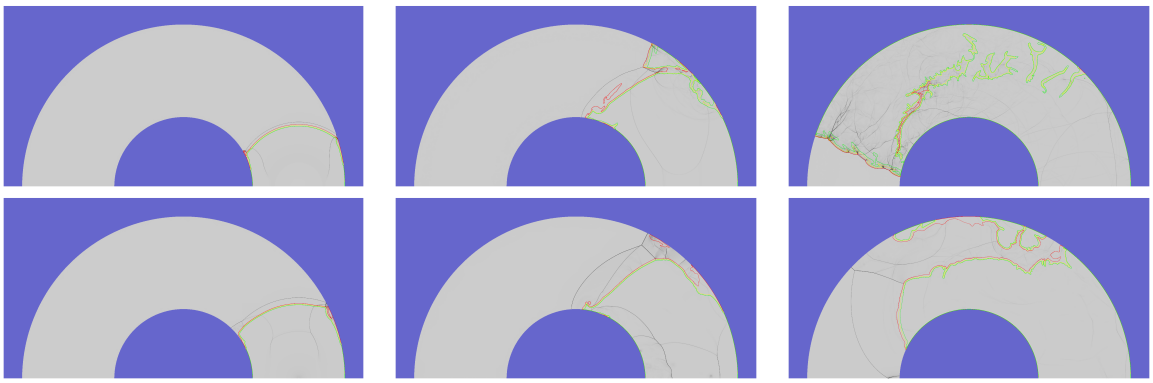

Figure 5: The evolution of the arc (top row) and spherical geometries (bottom row) with $E = 20$. Geometry and contours as in Fig. 2.

equator that accelerates the overall flow also potentially accelerates the reaction locally whereas the arc seems to decelerate in this region. This may again highlight how the reaction in the interior is important to impel the wave to propagate around the geometry but it appears harder to ignite the wave locally there and there is an absolute necessity for the outer transverse shock wave to achieve this (for our specific ignition scenario at least) in both geometries.

For $E = 20$, a further thermal sensitivity increase leads to more even dramatic initiation processes. For the arc, Fig. 5 (top row) shows how the transverse wave that forms on the outer contour where the front curvature is minimal is the primary agent to ultimately ignite the largely uncoupled flow in the interior of the explosive region. Large unreacted pocket again persists almost across the whole geometry. This is akin to the spherical case for $E = 15$. For the spherical case results shown in Fig. 5 (bottom row), it is clear that we have a total failure in initiating the wave. The explosive is largely unburnt across the geometry. Not even the wave reflection at the equator seems to generate sustained reaction.

4 Conclusion

The initiation dynamics resulting from a circular cross-section hot spot in two curved geometries of different dimensionality has been explored. In addition, this was done as a function of activation energy for a one-step Arrhenius gaseous explosive model. Larger activation energies tend to generate difficulties in initiating the wave for both a 2D arc and spherical geometry (i.e. relative to $E = 10$ which produces

prompt initiation and steady laminar flow in interior of this geometry). In particular, we see wave failure in the spherical geometry for a large enough activation energy ($E = 20$) and also partially burned pockets even for $E = 15$, an earlier onset relative to the arc geometry. While the cross-sectional area of the burnt region is equivalent between the two geometries, it is not evidently equivalent in terms of the initially burnt region in volume terms and so comparisons across these two geometries are quite exact. Nevertheless, there is some indication here that the three-dimensionality of the geometry and the additional curvature component for the spherical case may be contributing to an increase in difficulties initiating the wave. Further work will clarify the relative difficulties in initiation between the two geometries however by varying the size of the hot spot and also using the ZND flow to initiate the wave and help investigate the wave's persistence (or not) as function of geometry and activation energy.

References

[1] C. Chiquete and M. Short. Curvature effect on stabilization of cellular detonations in channel, circular arc and spherical shell geometries. *Proc. Combust. Inst.*, 40(1-4):105712, 2024.

[2] C. Chiquete, M. Short, and J. J. Quirk. The effect of curvature and confinement on gas-phase detonation cellular stability. *Proc. Combust. Inst.*, 37(3):3565–3573, 2019.

[3] C. A. Eckett, J. J. Quirk, and J. E. Sheperd. The role of unsteadiness in direct initiation of gaseous detonations. *J. Fluid Mech.*, 421:147–183, 2000.

[4] J.J. Erpenbeck. Stability of idealized one-reaction detonations. *Phys. Fluids*, 7:684–696, 1964.

[5] J.H.S Lee. *The detonation phenomenon*. Cambridge University Press, 2008.

[6] D. J. Lont, S. I. Jackson, C. Chiquete, and M. Short. The evolution of the velocity-curvature-acceleration relationship with activation energy for unstable gaseous detonations. In *AIAA SCITECH 2023 Forum*, page 1288, 2023.

[7] F. K. Lu and E. M. Braun. Rotating detonation wave propulsion: experimental challenges, modeling, and engine concepts. *J. Propul. Power*, 30(5):1125–1142, 2014.

[8] H. Nakayama, T. Moriya, J. Kasahara, A. Matsuo, Y. Sasamoto, and I. Funaki. Stable detonation wave propagation in rectangular-cross-section curved channels. *Combust. Flame*, 159:859–869, 2 2012.

[9] H. D. NG and J. H. S. LEE. Direct initiation of detonation with a multi-step reaction scheme. *J. Fluid Mech.*, 476:179–211, 2003.

[10] J.J. Quirk. *An adaptive grid algorithm for computational shock hydrodynamics*. PhD thesis, Cranfield, UK, 1991.

[11] J.J. Quirk. AMRITA - a computational facility (for CFD modelling). In H. Deconinck, editor, *29th Computational Fluid Dynamics*. von Karman Institute for Fluid Dynamics (1998), 1998.

[12] V. Raman, S. Prakash, and M. Gamba. Nonidealities in rotating detonation engines. *Annu. Rev. Fluid Mech.*, 55(1):639–674, 2023.

[13] M. Short, C. Chiquete, and J. J. Quirk. Propagation of a stable gaseous detonation in a circular arc configuration. *Proc. Combust. Inst.*, 37(3):3593–3600, 2019.

[14] M. Short and D.S. Stewart. Cellular detonation stability. part 1. a normal-mode linear analysis. *J. Fluid Mech.*, 368:229–262, 1998.